ACS OMEGA

Open Access

http://pubs.acs.org/journal/acsodf

Article

Treating Waste with Waste: Activated Bauxite Residue (ABR) as a Potential Wastewater Treatment

Fei Cheng, Jingya Pang, Scott Berggren, Himanshu Tanvar, Brajendra Mishra, and Maricor J. Arlos*

Cite This: *ACS Omega* 2024, 9, 45251−45262

Read Online

ACCESS | Metrics & More | Article Recommendations | Supporting Information

ABSTRACT: Bauxite residue (or red mud) is a highly alkaline waste generated during the extraction of alumina. As a result of the substantial accumulation of bauxite residue in tailings facilities, there is a growing interest in exploring the potential for reusing this material for other purposes. The main objective of this study is to evaluate the use of activated bauxite residue (ABR) for remediating oil sands process-affected water (OSPW) and as a supplement to municipal wastewater treatment through bench-scale, proof-of-concept studies. The ABR is produced through a reduction roasting process that alters the physicochemical properties of bauxite residue, resulting in the generation of potentially effective adsorbent media. The treatment performance via chemical and biological activity removals (cytotoxicity, estrogenicity, and mutagenicity) was also assessed. For OSPW, ABR treatment resulted in the effective removal of recalcitrant acid-extractable organics (AEOs), with kinetics following the pseudo-second-order and comparable adsorption capacity to other waste materials (e.g., petroleum coke). ABR also effectively reduced the estrogenicity and mutagenicity of OSPW, albeit cytotoxicity increased at higher dosages, possibly due to some components leaching out of the material (e.g., metals). For municipal wastewater, ABR treatment reduced fecal coliform concentrations (>99%), total phosphorus (up to 98%), total ammonia-nitrogen (63%), estrogenicity (nondetectable), and mutagenicity (nondetectable), especially in the primary effluent. The ultimate end use of ABR is for the recovery of valuable metals (especially iron) and as a construction material, but additional work is needed to optimize the dosage (currently in the g/L range) and maximize the use of ABR as an adsorbent prior to its subsequent uses.

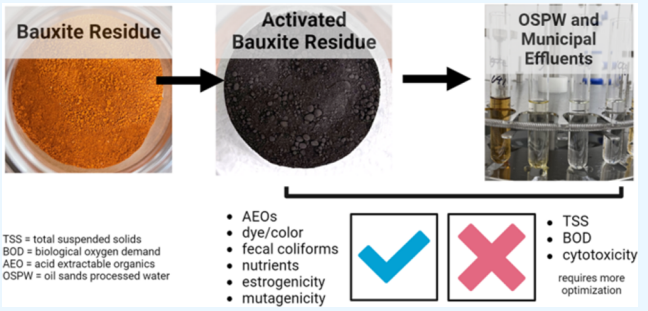

1. INTRODUCTION

Bauxite residue, or red mud, is a highly alkaline byproduct during alumina extraction (pH ranges from 12 to 13).[1] Depending on the ore quality and the extraction process, producing 1 tonne of alumina will generate 0.4−2 tonnes of bauxite residue.[2] The global production rate of bauxite residue has reached 150 million tonnes/year, with a utilization rate of only roughly 2%.[3] Besides occupying extensive land resources, the current management practice of stockpiling in tailings ponds risks spilling and releasing toxic metals into surrounding environments[4] as in the case of red mud slurry spill in Hungary due to a dam failure.[5] With the global drive toward sustainable development, a considerable amount of research has been conducted to explore the reuse potential of bauxite residue in various fields including construction, metallurgy, and environmental remediation. In construction, bauxite residue can be applied as a bulk material for roadbeds and landfill covers or as additives for building materials such as cement and geopolymers.[6−10] Due to the scarcity and rapid consumption of natural ores in metallurgy, the potential to recover valuable metals from bauxite residue has also become attractive (e.g., Fe, Ti, Al).[11−13] In environmental remediation, researchers have exploited the alkalinity, catalytic nature, and sorption capacity of bauxite residue for air, soil, and water treatment.[14−18]

Generated from Alberta oil sands surface mining and bitumen extraction, oil sands process-affected water (OSPW) is toxic to aquatic organisms and comprises a complex mixture of substances such as naphthenic acids (NAs), polycyclic aromatic hydrocarbons (PAHs), phenols, and heavy metals.[19,20] NAs are specifically considered one of the primary pollutants in OSPW.[19] The discharge of (un)treated OSPW into natural water bodies is currently prohibited, leading to accumulation of OSPW in tailings facilities.[21] A number of technologies have been shown to be effective in the removal of naphthenic acids, including adsorption-based processes.[22] Bauxite residue is an economical adsorbent alternative as it can remove a variety of pollutants such as dyes, phenols,

Received: July 19, 2024
Revised: October 22, 2024
Accepted: October 23, 2024
Published: November 2, 2024

pharmaceuticals, heavy metals, and ferricyanide[23−28] and recover phosphorus and nitrogen in municipal wastewater.[29] To date, the use of bauxite residue waste for the removal of NAs has never been explored.

In municipal wastewater treatment, adsorption processes via activated carbon (individually or in combination with ozonation) has been utilized to remove micropollutants including pharmaceuticals and personal care products (PPCPs) and other persistent, mobile, and toxic substances. PPCPs are present in wastewater effluents at low concentrations (ppb to ppt levels) but have the potential to induce biological activities (e.g., estrogenicity) toward exposed aquatic organisms. Full-scale implementations of activated carbon in wastewater have been done in Switzerland,[30,31] Sweden,[32] and Germany[33] to improve PPCP removals (∼80% removals). Hence, as the consumption of micropollutants continues to rise and global attention shifts toward water reuse, the utility of additional treatment operations (such as adsorption) to improve the municipal wastewater effluent quality will likely be adopted more widely.

This study evaluated the potential of implementing activated bauxite residue (ABR) as a cost-effective adsorbent material for the OSPW and municipal wastewater treatment. ABR underwent a reduction roasting process, resulting in the magnetization of bauxite residue, generation of a porous surface structure, and reduction in pH. As a consequence of this process, ABR is hypothesized to have an improved adsorption capacity, further highlighting its versatility for a variety of applications, including wastewater treatment. In this study, ABR properties were first characterized to gain insights into its adsorbent behavior. Proof-of-concept, bench-scale experiments were then completed to evaluate the performance of this method in removing acid-extractable organics (AEOs) in OSPW and its associated biological activity (cytotoxicity, estrogenicity, and mutagenicity). Several types of municipal wastewater effluents (primary-, secondary-, and UV-treated effluents) were tested to evaluate the removal of key water quality parameters and biological activity, especially estrogenicity.

2. MATERIALS AND METHODS

2.1. Sample Collection and Materials. The ABR material was produced using the methods described by Gostu.[34] Briefly, raw bauxite residue was blended with a stoichiometric amount of carbon and subsequently subjected to thermal treatment in a rotary calciner under an inert atmosphere of nitrogen gas. The reduction roasting was performed in the range of 500−600 °C with 30 min residence time. The OSPW sample was obtained from an oil sands tailings pond operator in northern Alberta. Three types of municipal wastewater samples were collected after the biological nutrient removal (BNR) (primary effluent [PE]), the secondary clarifier (secondary effluent [SE]), and the disinfection unit (UV-treated [Post-UV]) from a municipal wastewater treatment plant in Alberta. All samples were stored in amber glass bottles at 4 °C before testing (holding time <5 d).

Acetic acid (≥99.7%), ethyl acetate (≥99.5%), and dichloromethane (DCM) (≥99.8%) were purchased from Sigma-Aldrich. Hydrochloric acid (HCl, diluted in ultrapure water to 1N and 0.1 N) and methanol (≥99.9%) were purchased from Fisher Scientific and diluted in ultrapure water (1N, 0.1N). Ultrapure water was produced by a Milli-Q IQ 7000 purification system with a resistivity of 18.2 MΩ·cm (25 °C) and total organic carbon (TOC) ≤5 ppb. Information on bioassay reagents (cytotoxicity, estrogenicity, and mutagenicity) is found elsewhere.[35]

2.2. Material Characterization. The microscopic properties of ABR were investigated via scanning electron microscopy (SEM) using a Zeiss EVO MA 10. Before analysis, ABR particles were mounted on carbon-taped stubs and coated with gold for 100 s at 150 mT using a Denton gold sputter unit. Energy-dispersive X-ray (EDX) analysis was also performed with SEM to determine the elemental composition of ABR, which complemented the inductively coupled plasma optical emission spectroscopy analysis (ICP-OES, PerkinElmer Optima 8000). The total organic carbon (TOC) was analyzed using the LECO carbon analyzer as interference during SEM-EDX sample preparation may influence the carbon content results. The magnetic properties were assessed using vibrational sample magnetometry (VSM) as described elsewhere.[36] Phase identification was conducted via X-ray diffraction (XRD) using a Bruker XRD D8 Discover, with a copper source and an X-ray throughput of 40 kV and 30 mA (2θ = 4−80°). Brunauer−Emmett−Teller (BET) surface area, total pore volume, and density functional theory (DFT) pore size distribution were obtained by the gas adsorption/desorption method. The sample was first outgassed for 4 h at 200 °C, and the analysis was conducted at 77 K with nitrogen using an Autosorb-iQ (Anton-Paar, Canada). Samples were also sent to the University of Calgary (Research Instrumentation and Technical Support Lab) for ζ-potential measurements (determining surface charge).

2.3. Adsorption Kinetics and Isotherm. The kinetic experiments started with mixing 1800 mL of OSPW with 50 g/L ABR at 120 rpm using the jar tester (VELP FC 4S Flocculation Stirrer) for 72 h. A total of 20 water samples (10 mL) were collected at different time points from 0 to 72 h, filtered through sterile 0.45 μm nylon syringe filters (Basix Syringe Filters, PVDF), and acidified to a pH of ∼2 using 1 N HCl for solid-phase extraction (SPE, Section 2.5) with filtrate volumes from 7.1 to 9.5 mL. The concentration of AEOs was measured via Fourier transform infrared spectroscopy (FTIR see ref 35), and the data were fitted to the linearized forms of pseudo-first-order (eq 1) and pseudo-second-order (eq 2) kinetic models described by[37]

$$\log(q_e - q_t) = \log q_e - \frac{k_1}{2.303}t \quad (1)$$

$$\frac{t}{q_t} = \frac{1}{k_2 q_e^2} + \frac{t}{q_e} \quad (2)$$

where q_t is the mass of AEOs adsorbed per gram of ABR at time t, calculated by $\frac{(C_0 - C_t)V}{M}$, in which C_0 is the initial concentration of AEOs, C_t is the concentration of the AEOs at t, V is the volume of OSPW, and M is the mass of ABR added, q_e is the mass of the AEOs adsorbed at equilibrium, and k_1 and k_2 are equilibrium rate constants for the pseudo-first-order and pseudo-second-order kinetic models, respectively.

The isotherm experiment was performed by mixing different ABR doses, ranging from 0 to 100 g/L, with 40 mL of the OSPW in 50 mL glass conical tubes. The tubes were placed horizontally in a shaker at 150 rpm for 2 days, and the solution was left sitting for 2 h to allow settling of particles. The supernatant was then prepared as described above. The data

https://doi.org/10.1021/acsomega.4c06699
ACS Omega 2024, 9, 45251−45262

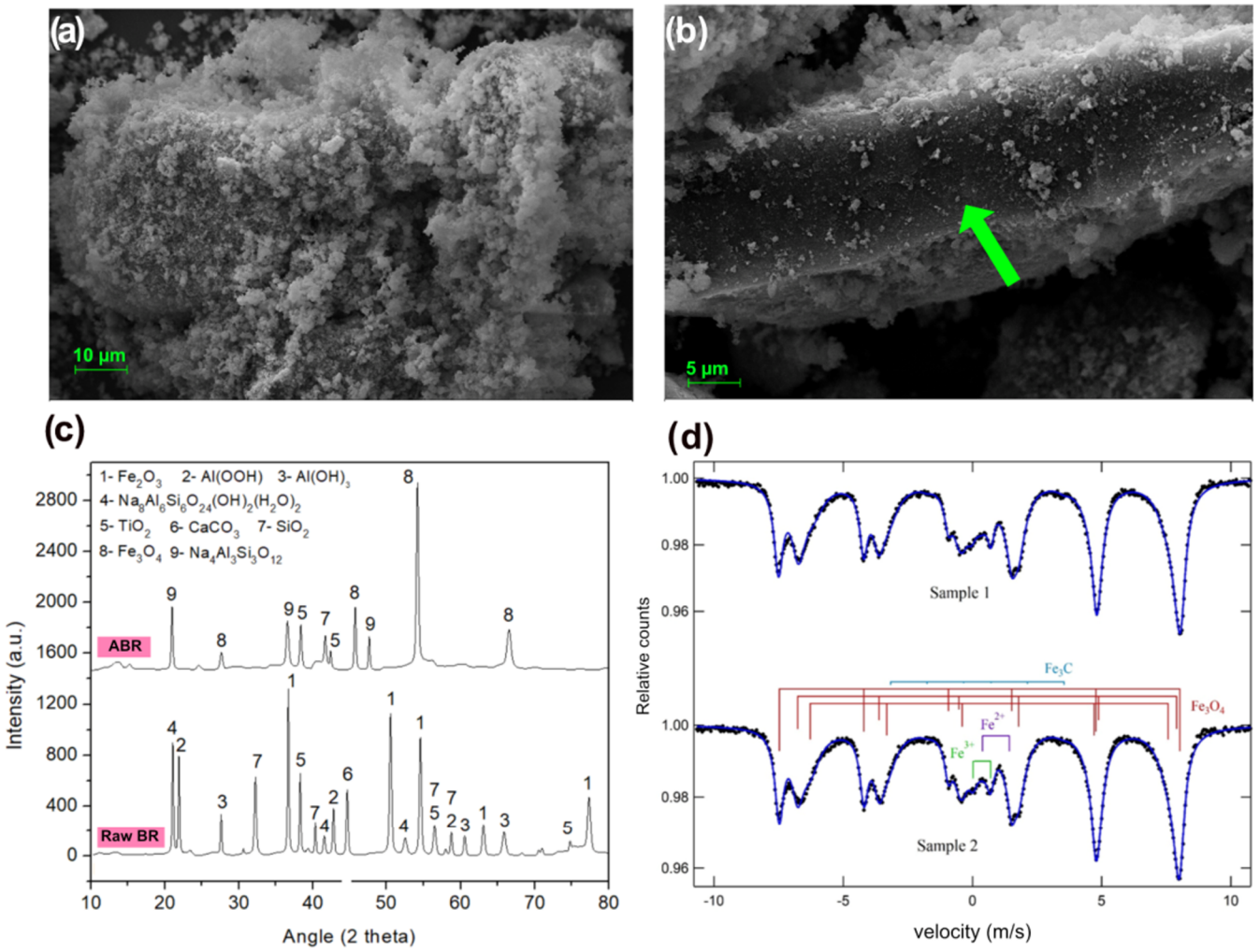

Figure 1. Scanning electron microscopy (SEM) images of activated bauxite residue (ABR) particles: (a) metal-rich and (b) carbon-rich (green arrow). Images taken at a magnification of 1000× (a) and 2000× (b) and a working distance of 7.3 mm. (c) X-ray diffraction (XRD) spectrum of ABR (bulk sample). (d) Mössbauer spectroscopy to characterize different Fe species in ABR. Sample 1: Fe as Fe_3O_4 = 86%; Fe as Fe^{2+} = 8%; Fe as Fe^{3+} = 4%; and Fe as Fe_3C = 2%; Sample 2: Fe as Fe_3O_4 = 87%; Fe as Fe2+ = 7%; Fe as Fe^{3+} = 5%; and Fe as Fe_3C = 1%. The statistical uncertainty in the Fe fractions is about ±1%.

obtained were fitted to the Langmuir (eq 3) and Freundlich (eq 4) isotherm models

$$q_e = \frac{K_L Q_m C_e}{1 + K_L C_e} \quad (3)$$

$$q_e = K_F C_e^{1/n} \quad (4)$$

where C_e is the concentration of AEOs at equilibrium, K_L and Q_m are constants for the Langmuir isotherm model: Q_m is the maximum adsorption capacity and K_L is the adsorption affinity coefficient, and K_F and n are Freundlich isotherm constants: K_F is the adsorption affinity coefficient and n is the nonlinear index.

2.4. General Bench-Scale Water Treatment Method. Different dosages of ABR (0, 20, 50, and 100 g/L) were mixed with 500 mL of OSPW at 120 rpm for 24 h by using the jar tester. During treatment, the water was highly alkaline, and each ABR dosage (20−100 g/L) raised the sample pH from ∼7.8 to 9.8, 10.6, and 11.3, respectively. After 24 h, the solution was neutralized to pH 6.5−8.5 using acetic acid and was allowed to settle for 30 min. The samples were filtered using a 1 μm-pore hydrophilic glass fiber filter (Sigma APFB04700) and acidified to ∼ pH 2 as above. The filtrate was divided into smaller volumes for extraction separately via SPE: (1) 50 mL for FTIR and (2) 50−100 mL for *in vitro* bioassays.

Following a procedure similar to that above, 1.8 L of municipal wastewater (primary-, secondary-, and post-UV-treated effluents) was mixed with 0, 50, and 100 g/L ABR at 120 rpm for 24 h. An increase in pH was also observed during treatment, from ∼7 to 11.7 and 12.2 for 50 and 100 g/L ABR, respectively, followed by neutralization (similar to OSPW) prior to submitting to a certified analytical lab (Bureau Veritas, Edmonton) for the analyses of total suspended solids (TSS), biological oxygen demand (BOD), total ammonia-N, total phosphorus, fecal coliform, and dissolved metals. The same experiment was completed to obtain another sample volume of 1 L for *in vitro* bioassays.

The experiments were conducted with n = 1, which is recognized as a limitation. However, this study was exploratory in nature and aimed at generating a proof of concept for ABR use in wastewater treatment. Our goal was to provide preliminary data for future studies, in which larger replication

https://doi.org/10.1021/acsomega.4c06699
ACS Omega 2024, 9, 45251−45262

efforts will be implemented. Limitations in sample volumes required for chemical analyses and *in vitro* bioassays also contributed to this decision. Furthermore, instead of conducting multiple experimental replication, the focus was on generating more data points over the experiment duration, especially the kinetic experiments where ∼30 data points were collected to improve curve fitting (e.g., Figure 4a). For the *in vitro* bioassays, previous work from our lab (e.g., Barrow et al.[35]) found that single-replication design is sufficient given the assay's established replicability and reproducibility.

2.5. Sample Preparation: Solid-Phase Extraction. The SPE was completed for FTIR and *in vitro* bioassays and followed the procedure in Barrow et al.[35] with slight modifications on sample volumes and cartridge sorbent mass. Briefly, the Oasis HLB 6 cm^3 cartridges with a sorbent mass of either 150 or 500 mg were preconditioned with 5 mL of methanol followed by 10 mL of ultrapure water. OSPW samples that were <50 mL were extracted using 150 mg of sorbent; OSPW samples of >50 mL and the 1 L municipal wastewater samples were extracted using 500 mg of sorbent. Samples were introduced into the cartridges either by vacuum (for volumes >50 mL) or slow pipetting (for volumes <50 mL). Following sample introduction, the cartridges were rinsed with 10 mL of ultrapure water (pH 2) and were dried under vacuum for at least 45 min and eluted with 5 mL of methanol and 5 mL of 1:1 methanol:ethyl acetate (v/v). The eluent was evaporated to dryness under gentle nitrogen stream blowing and a water bath at 30−35 °C. For FTIR, the samples were kept dried until analysis to prevent the potential loss of the DCM solvent through volatilization; for *in vitro* bioassays, the samples were reconstituted with 1 mL of methanol. All SPE extracts were stored at −20 °C in the dark.

2.6. *In Vitro* Bioassays to Assess Biological Activity during Treatment. The determination of cytotoxicity, estrogenicity, and mutagenicity utilized the same reagents, procedure, and data analysis as Barrow et al.[35] Briefly, cytotoxicity was determined by the percent inhibition on *Aliivibrio fischeri* after exposure to the sample using the Biotox-Lumoplate kit (Environmental Biodetection Products Inc. [EBPI]). Estrogenicity was measured using the yeast estrogen screen (YES) assay procedure described elsewhere.[38] The detection of mutagenicity relies on the SOS response of *Salmonella typhimurium* to DNA damage and was measured using the Umu-Chromo (gene) kit also from EBPI. Briefly, the concentration causing 10% inhibition after 15 min of exposure (IC_{10}) for cytotoxicity, the concentration exhibiting a 10% estrogenic effect (EC_{10}), and the concentration imposing an induction ratio of 1.5 ($EC_{IR1.5}$) were calculated and compared against treatments. The concentration was expressed as the relative enrichment factor (REF), which accounts for both the sample extraction factor and the dosing factor used for bioanalysis. For cytotoxicity, the data were represented as $1/1C_{10}$ and estrogenicity and mutagenicity REFs were then converted to BEQs (see Barrow et al.[35]) based on the reference compound (i.e., 17-β estradiol (E2) equivalents (eq) for estrogenecity and 4-nitroquinoline 1-oxide (4-NQO) eq for mutagenicity).

3. RESULTS AND DISCUSSION

3.1. Material Characterization. SEM-EDX results[TC4] (Figure 1a,b) suggest the presence of unevenly sized particles with variable morphologies and surface characteristics. EDX analysis of the particle depicts the presence of residual carbon species from the thermal treatment process, with the bulk ABR sample containing about 1.33% organic carbon (Table S1b). When SEM-EDX was performed on individual particles (i.e., not the bulk material), the presence of two different types of particles in ABR was observed (Table S1a): (1) metal-rich (containing ∼42% metal and 16% carbon by weight) and (2) carbon-rich (containing ∼8% metal and 77% carbon). The composition of the metal-rich ABR particle is similar to raw bauxite residue (i.e., not thermally treated), which contains 4.5−50.6% Fe, 4.4−16.1% Al, 2.2−14.9% silicon (Si), 1.0−7.8% sodium (Na), 0.4−16.7 calcium (Ca), and 1.0−5.3% Ti.[39] Note that while there are two types of particles present in the bulk sample, it only contains a small amount of carbon (i.e., <2%) and is present in either form of iron carbide (i.e., metal-rich) or unreacted carbon (i.e., carbon-rich) during the reduction roasting process. The bulk chemical analysis of ABR determined from ICP-OES further shows the presence of other substances, including 1.78% Ca, 7.68% Si, 3.343% Ti, 8.86% Na, 37.82% Fe, and 11.81% Al (Table S1b).

The XRD analysis (Figure 1c) of the raw bauxite residue and ABR further indicates differences in the composition after the reduction roasting process. For instance, the raw bauxite residue consists of hematite (Fe_2O_3), boehmite (Al(OOH)), gibbsite ($Al(OH)_3$), sodium aluminum silicate hydrate/sodalite ($Na_8Al_6Si_6O_{24}(OH)_2(H_2O)_2$), calcium carbonate ($CaCO_3$), quartz ($SiO_2$), and rutile ($TiO_2$) phases. The reduction roasting process used to produce ABR resulted in the partial reduction of hematite to magnetite (Fe_3O_4) and converted the sodalite and other Al-bearing phases into sodium alumino silicate ($Na_4Al_3Si_3O_{12}$). No apparent peaks corresponding to hematite were found in the XRD spectrum of the ABR, depicting complete conversion. ABR also exhibits magnetic characteristics due to the presence of magnetite as a major constituent, with the vibrating-sample magnetometer (VSM) analysis showing high magnetization properties with a saturation magnetization of 25.19 emu/g and coercivity of 267.74 Oe.

Mössbauer analysis was additionally performed to determine the fraction of different Fe species in the ABR sample. Figure 1d shows the spectra and fits for the two samples, indicating that magnetite (Fe_3O_4) is the dominant species. The stick diagrams show the various phases found in the fitting. The Fe_3O_4 resonance is quite broad and requires three subspectra for a good fit. This result indicates either a small grain size causing some magnetic relaxation or a large amount of impurities in the magnetite. Also, there are two nonmagnetic subspectra labeled Fe^{3+} and Fe^{2+} and these may be superparamagnetic spectra due to the very small grain size Fe_3O_4 or some unknown paramagnetic phase(s) containing Fe^{3+} and Fe^{2+}. Finally, there is evidence for a small amount of cementite at <1% (Fe_3C).

The presence of multiple metal oxides with high specific surface area, magnetic properties, functional groups, chemical stability under moderate pH conditions, and surface characteristics makes ABR a potential adsorbent for the removal of many contaminants in the water column, and the presence of magnetite suggests that it can be recovered after use in wastewater treatment (outside the scope of this study). It is further hypothesized that a combination of physical (e.g., van der Waal forces) and chemical sorption (i.e., adsorbates from covalent or ionic bonds with the surface) is a possible mechanism given the complexity in ABR's composition and surface chemistry.

https://doi.org/10.1021/acsomega.4c06699
ACS Omega 2024, 9, 45251−45262

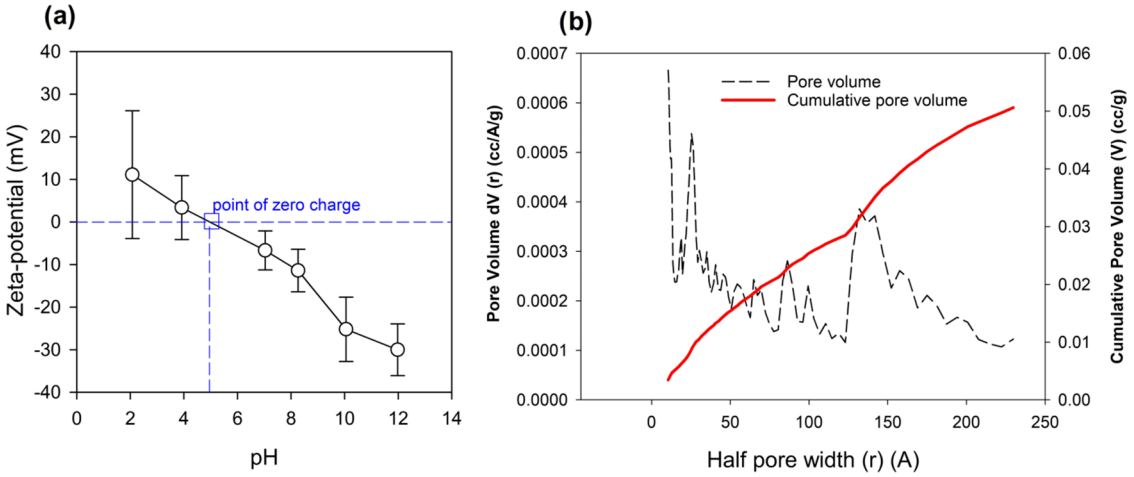

Figure 2. Point of zero charge for the activated bauxite residue based on ζ-potential measurements (a). Pore size distribution obtained via density functional theory (Autosorb) suggests mesoporous characteristics of ABR (pore mostly 2−50 nm in diameter) (b). *y*-axis of the pore size distribution curve $dV(r)$ refers to the volume of pores with radii between r and $r + dr$. 1 Å = 0.1 nm.

The surface charge of the adsorbent can also play a role during the adsorption process. The point of zero charge (PZC) for ABR was found to be ∼ pH 5 (Figure 2a), suggesting that ABR is positively charged below this pH and negatively charged for any pH > 5. Depending on the type of bauxite residue, the PZC (i.e., pH where the net charge of the material is zero) has been observed to vary from 5.98 to 8.70.[40,41] Given that many organic contaminants are charged/ionizable (e.g., pharmaceuticals, personal care products), surface charge can impact mass transfer to ABR. Bjelopavlic et al.[42] indicated that the total free energy of adsorption of organic matter onto an adsorbent (i.e., activated carbon) is a combination of electrostatic and specific free energies, with electrostatic interactions comprising both Coulombic and dipole interactions. Electrostatic attraction and repulsive interactions of organics among each other and onto the adsorbent's surface are highly dependent on pH.

ABR has a BET surface area of 25.1 m^2/g, and the total pore volume is 0.137 cm^3/g. DFT pore size distribution (Figure 2b) shows that ABR contains pores with diverse sizes ranging from 2 to 46 nm, which can be categorized as mesopores (pores with 2−50 nm diameter).[43] Compared to bauxite residue-based adsorbents in the literature (Table 1), the BET surface area of ABR is in the same order of magnitude as raw bauxite residue and bauxite residue treated with salt, acid, and/or heat. However, the ABR utilized in this study has a higher total pore volume, ∼1.4 to 6.9 times those treated with salt, acid, and/or heat, possibly due to the difference in the pretreatment process or raw material. The thermal process utilized for the production of ABR likely resulted in the generation of a porous surface due to the gas−solid reaction taking place during the reduction of hematite to magnetite ($2Fe_2O_3 + CO \rightarrow 2Fe_3O_4 + CO_2$). The thermal treatment process also reduced the alkalinity of bauxite residue, thereby making it more suitable for practical application as an effective adsorbent.

It appears that more superior surface area and pore volumes were observed by others (Table 1) when additional modification (e.g., hydrochloric acid [HCl] + ammonium hydroxide [NH_4OH]) is incorporated or bauxite residue is created as a composite material (i.e., with carbon). However, it is important to mention that some modifications involve complete dissolution of bauxite residue in a concentrated hydrochloric acid solution followed by precipitation of the dissolved material by ammonium hydroxide, which can change the composition of the bauxite residue significantly.

Table 1. BET Surface Area and Total Pore Volume of Raw and Treated Bauxite Residue from the Literature

treatment type	BET surface area (m^2/g)	total pore volume (cm^3/g)	references
raw	22.9 ± 15.6[a]	0.04 ± 0.02[a]	[b]
Neutralization with Salt			
gypsum	12.8	0.03	44
seawater	13.8	0.03	44
Acid Treatment			
hydrochloric acid (HCl)	28.5	0.08	45
nitric acid (HNO_3)	38.2	0.07	45
HNO_3	31.9	0.06	46
Heat Treatment			
300 °C	18.0	0.02	46
800 °C	10.1	0.03	47
Acid + Heat Treatment			
HCl + 700 °C	33.8	0.09	45
HNO_3 + 700 °C	33.3	0.10	45
Acid + Heat + Ammonium Hydroxide (NH_4OH) Treatment			
HCl + NH_4OH	207	0.31	48
HCl + NH_4OH + 200 °C	381	0.90	48
Composited with Other Material			
sucrose-based carbon	105	0.22	49
polystyrene microspheres	232	0.27	50

[a]Mean ± standard deviation. [b]Not completed in this study but compiled from the literature (see refs 44−50).

The surface area was also not comparable to commercially available powdered activated carbon (PAC), which can have a surface area of >1000 m^2/g and exceptional microporosity and mesoporosity.[51] Nonetheless, our preliminary experiment on the removal kinetics and adsorption isotherms of methylene blue (organic dye) by ABR further showed that its adsorption capacity (∼1 mg/g) (Supporting Information, SI-C, Figure S3, Tables S3, and S4) is comparable to Martins et al.[46] who utilized bauxite residue for dye removal using bauxite residue from Brazil. However, our adsorption capacity was much lower compared to residues composited with sucrose-based carbon

https://doi.org/10.1021/acsomega.4c06699
ACS Omega 2024, 9, 45251−45262

(23 and 48 mg/g)[49] and acid-treated[48] (SI, Table S4). This result was not surprising as bauxite residues that were composited with carbon elicit high surface area and pore volume and have more available sorption sites. However, this study still highlights that the low material cost and abundance of ABR make it a ubiquitous, less expensive alternative even if a higher dosage is required, with bench-scale (batch tests) bauxite residues also reporting dosages ranging from 1 up to 500 g/L[44] (Table S4). Hence, further optimization of the material (i.e., pretreatment as indicated in Table 1) was not deemed necessary at this stage as the reduction roasting process was also meant to facilitate the fast recovery of magnetite in the "spent" ABR. A subsequent process such as centrifugation has been considered a feasible separation process after wastewater treatment as ABR can be sent elsewhere to recover magnetite, which can be a valuable metallic ore (not covered in this study). Therefore, it is deemed appropriate to assess the potential of the current ABR material to remove pollutants and biological activities from industrial and municipal wastewater treatment plants as discussed subsequently below. Note that the dosages employed were an order of magnitude higher than typical adsorbent (i.e., PAC) dosages. Note that this study is focused on a proof-of-concept approach to understand the adsorption capacity and removal kinetics as they are related to ABR materials, with optimization currently underway.

3.2. Post-treatment Neutralization. ABR elevates the matrix pH and therefore necessitates post-treatment neutralization to meet effluent discharge standards. There is also a potential for metal ions to leach out of the material, especially aluminum (Al), as it is available in its dissolved form at alkaline pH conditions. Indeed, Al increased from 8.2×10^{-3} to 100 mg/L during the 50 g/L ABR treatment of OSPW, and a similar outcome was observed during a leaching test in ultrapure water and 5% tertiary-treated effluent (Figure 3). Neutralizing the solution to pH 7 with acetic acid dramatically reduced Al by 5000 times (e.g., from 190 to 0.037 mg/L in ultrapure water). Also, this effectively controlled the Al releases in treated municipal wastewater effluents as evident in the minimal increase of Al post-treatment neutralization (Figure 3). The choice of acetic acid mitigates potential issues from the release of other inorganic substances (such as chloride from hydrochloric acid), which could further impact aquatic environments.

3.3. Treatment of OSPW. *3.3.1. Adsorption Kinetics and Equilibrium Experiments.* The adsorption equilibrium of AEOs (50 g/L ABR) was obtained after ~4 h, with a maximum removal of 50% (Figure 4a). The data did not follow the pseudo-first-order kinetic model well (SI-D) but was well described by the pseudo-second-order kinetic model (Figure 4a,b) based on their linear regression R^2 values (R^2 = 0.276 and R^2 = 0.992, respectively). From this model, the pseudo-second-order kinetic parameters derived were 0.24 and 0.15 g/mg/min for q_e and k_2, respectively. This adsorption process is also similar to our preliminary assessment of methylene blue (organic dye) sorption on ABR (please see SI-C).

When the adsorption kinetics data follow the pseudo-second-order kinetic model, it is assumed that the rate-limiting step is chemisorption, which suggests that the adsorption rate does not depend on the adsorbate concentration (i.e., target pollutant) but on the adsorption capacity of the material (i.e., available adsorption sites).[37] Mandal et al.[52] and Martins et al.[46] also found that the removals of phenols and dyes by

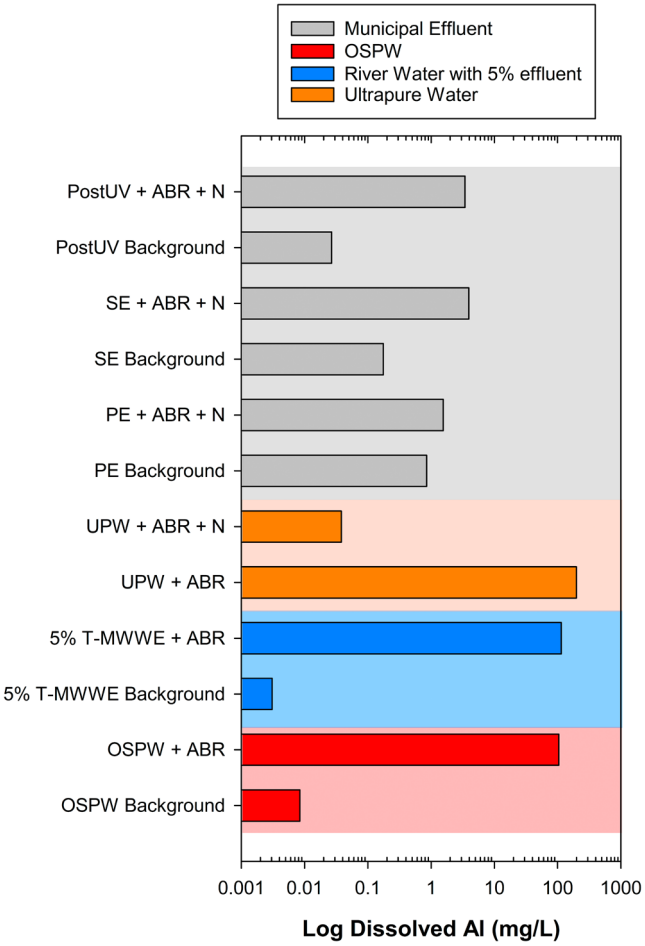

Figure 3. Impact of neutralization on reducing the leaching of dissolved Al from ABR during treatment. Post-UV = disinfected effluent; SE = secondary effluent; PE = primary effluent, UPW = ultrapure water; and T-MWWE = tertiary-treated effluent from a different WWTPs. ABR = activated bauxite residue, *N* = neutralized; and OSPW = oil sands process water. Other metal ions are found in SI-E and Tables S7−S11.

bauxite residue adsorbents follow the pseudo-second-order kinetic model, suggesting similar adsorption kinetics for other organic substances.

ABR has performance similar to those of other waste-based adsorbents such as petroleum coke and biochar. Bhuiyan et al.[53] generated biochar from a variety of sources and obtained adsorption capacities ranging from 0.04 to 0.59 mg/g, and Zubot et al.[54] examined the use of petroleum coke and found its adsorption capacity to be 0.16 mg/g (Table S6), similar to what was obtained in this study (0.24 mg/g). Considering that the use of petroleum coke for OSPW treatment was recently field-piloted,[55] it is therefore practical to assess the application of ABR in larger scale settings using the adsorption kinetics derived in this study.

For an ABR dosage of 15−60 g/L, the parameters obtained from the Langmuir isotherm model fitting were 0.0081 L/mg (K_L) and 1.84 mg/g (Q_m) (Figure 4c). The Freundlich isotherm parameters were 0.023 mg/g·(L/mg)$^{1/n}$ (K_F) and 1.24 (n). The data followed the Langmuir isotherm model (R^2 = 0.8415) slightly better than the Freundlich isotherm model (R^2 = 0.8285). Note that these R^2 values are relatively low (i.e., <0.9000), suggesting that the adsorption between the OSPW and ABR is complex, likely influenced by surface heterogeneity

https://doi.org/10.1021/acsomega.4c06699
ACS Omega 2024, 9, 45251−45262

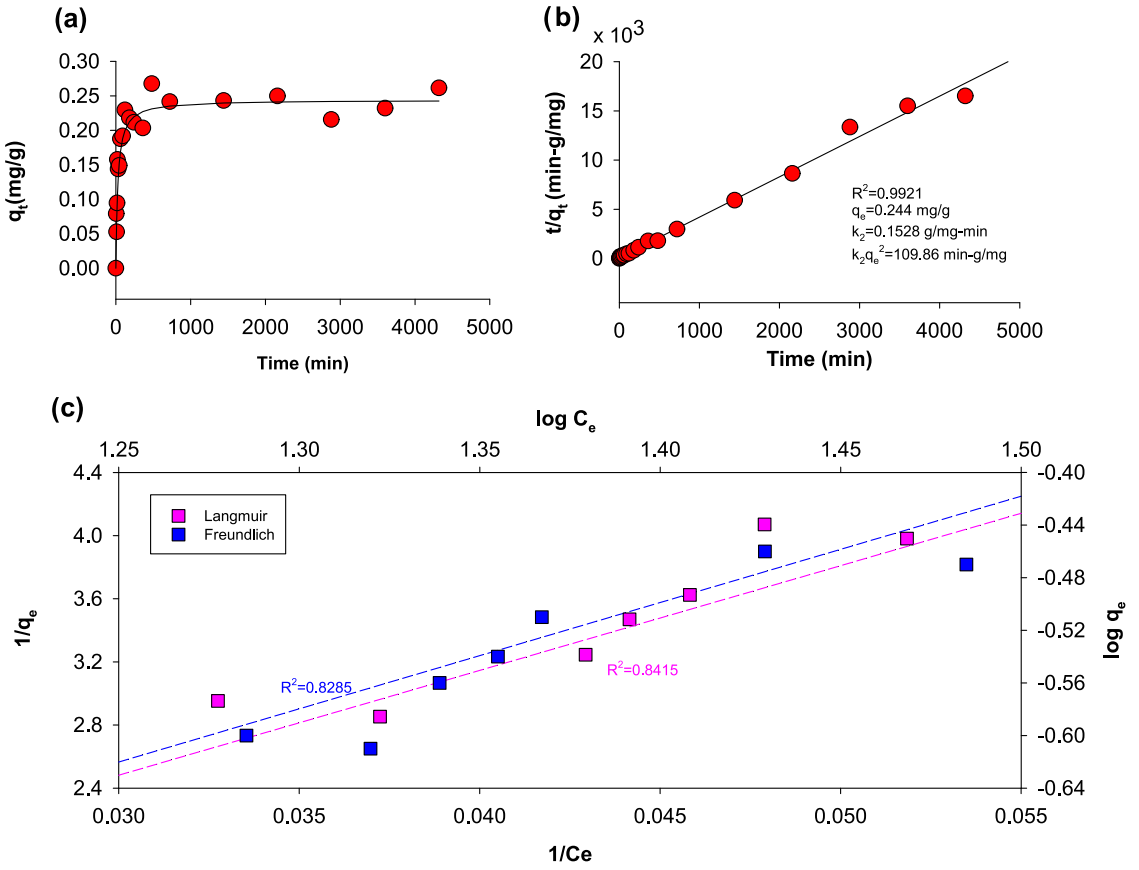

Figure 4. (a) Concentration of adsorbed acid-extractable organics (AEOs) obtained during the kinetic study; (b) pseudo-second-order kinetic model fit; and (c) isotherm fitting via Langmuir and Freundlich isotherms based on equilibrium concentrations derived dosages ranging from 15 to 60 g/L.

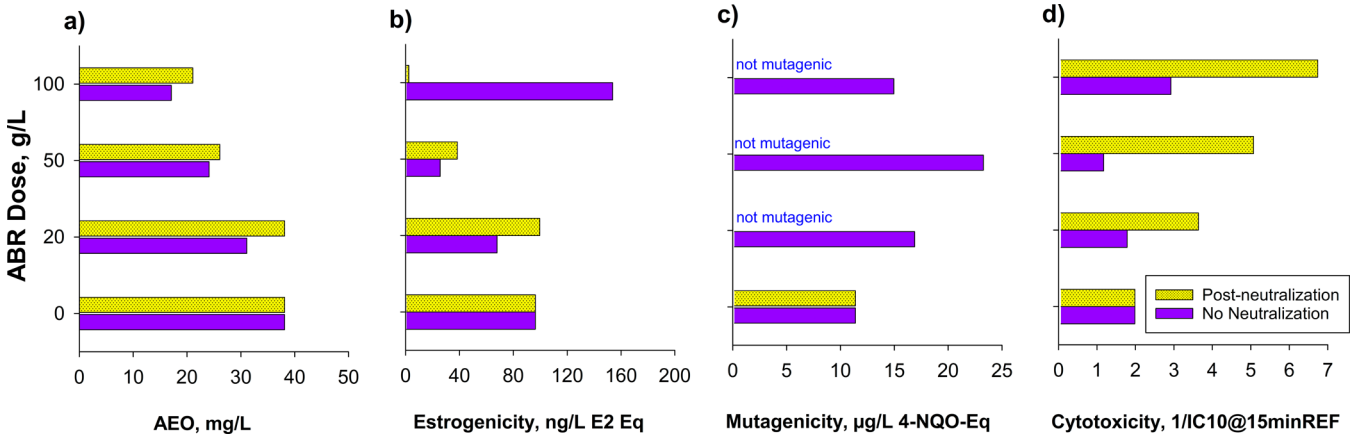

Figure 5. Quality of the ABR-treated oil sands process-affected water (OSPW): (a) acid-extractable organics (AEOs), (b) estrogenicity, (c) mutagenicity, and (d) cytotoxicity after the treatment with 0, 20, 50, and 100 g/L ABR doses. Note that the results of estrogenicity and mutagenicity are expressed as bioanalytical equivalents as it relates to their respective assay (i.e., estradiol equivalents (E2 equiv) for estrogenicity and 4-nitroquinoline oxide equivalents (4-NQO-eq) for mutagenicity). The larger the BEQ value, the higher the toxicity. Cytotoxicity is normally represented as IC10 (REF), but here, it is represented as 1/IC10 for a straightforward comparison of toxicity across all assays (i.e., higher 1/IC10 suggests higher toxicity).

and nonideal behaviors that are not adequately captured by these isotherm models. However, since the pseudo-second-order kinetic models indicate potential for chemisorption, it is therefore possible that the AEO sorption on the ABR follows the Langmuir isotherm. As chemisorption tends to be more specific (i.e., linked to chemical bonding), the pollutant will usually occupy specific adsorption sites only, creating a monolayer consistent with the Langmuir isotherm assumption. Furthermore, ABR is heterogeneous, and therefore, the metal-rich and carbon-rich particles likely exhibited different removal mechanisms. Nonetheless, the derived maximum adsorption capacity (Q_m) for the ABR was six times higher than the value derived for petroleum coke (0.39 mg/g),[54] suggesting that

https://doi.org/10.1021/acsomega.4c06699
ACS Omega 2024, 9, 45251−45262

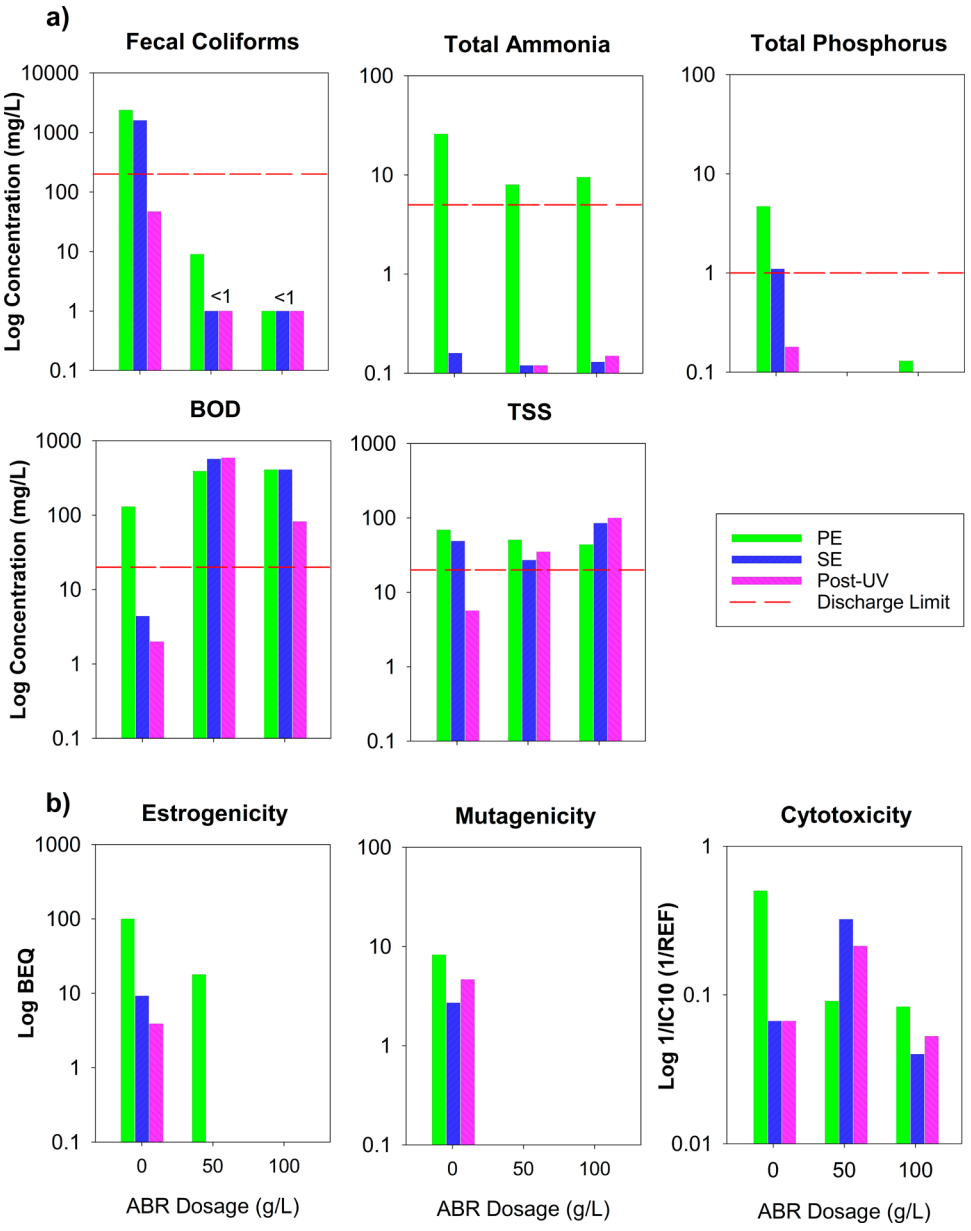

Figure 6. Improvement of water quality after activated bauxite residue (ABR) treatment. (a) Selected parameters and their discharge limits for WWTP A. (b) Removal of biological activity. PE = primary effluent; SE = secondary effluent; BEQ = bioequivalents expressed as estradiol (E2) equivalents (eq) for estrogenicity, and 4-NQO-eq for mutagenicity; REF = relative enrichment factor. Cytotoxicity is represented as 1/IC10 for a straightforward assessment of toxicity across all assays (i.e., higher 1/IC10 suggests higher toxicity). n.a. = no activity.

there is potential for ABR to be utilized in OSPW treatment similar to the petroleum coke.

3.3.2. Biological Activity Assessment of Treatment Efficiency. Complementary to chemical analysis, *in vitro* bioanalysis was employed to (1) determine additional toxicity contributed by ABR given its relatively high baseline toxicity and (2) assess the removal of toxicity from target water matrices that are known to have biological activity via these assays (cytotoxicity, estrogenicity, and mutagenicity). AEO concentrations declined with an increasing ABR dosage irrespective of the neutralization (Figure 5). Post-treatment neutralization at 50 and 100 g/L ABR showed removals of 32 and 45%, respectively, and these removals were slightly lower than ABR treatment without neutralization (37 and 55%). Nonetheless, ABR effectively removed AEOs from OSPW with efficiencies similar to that of biochar and petroleum coke.[53,54]

Untreated OSPW (0 g/L) showed observable *in vitro* biological activity as what had been observed in prior studies.[20,56] The removal of estrogenicity also corresponds to AEO removals (Figure 5b,c). This result supports the finding by Yue et al.[57] where they reported a degradation of 40% organics in the OSPW's acid-extractable fraction, which led to a removal of 22% in the YES assay using a biofilm reactor. ABR treatment also resulted in the effective removal of mutagenicity (Figure 5c) where bioanalytical equivalents were reduced from 11.2 μg/L 4-NQO-eq to "not mutagenic" for all three dosages tested, possibly related to the removal of mutagenic AEOs (or NAs). However, this was not the case for cytotoxicity, as it was observed to increase with increasing dose (Figure 5d). The 1/IC10 of the untreated OSPW increased from 1.9 to 3.6, 5.0, and 6.8 1/REF after the treatment of 20, 50, and 100 g/L ABR, respectively. This increase in toxicity may be due to the release

https://doi.org/10.1021/acsomega.4c06699
ACS Omega 2024, 9, 45251−45262

of metals/salinity and was intensified with the increased dosage and led to the formation of harmful metal complexes with OSPW constituents.

Domingues et al.[15] also utilized a combination of chemical and biological analyses to evaluate the efficiency of bauxite residue catalysts for olive mill wastewater treatment. Similarly, they observed an increase in toxicity despite the removal of phenolic acids and related this toxicity to the residual hydrogen peroxide concentration. Their work together with our study advocates the use of bioanalytical tools for water quality assessment to compensate for the shortcomings of chemical analysis (e.g., inability to detect the mixture effect, transformation byproducts, and unknown contaminants). More specifically, a battery of *in vitro* bioassays (as opposed to only using a single toxicity assay) is a good assessment tool to use, given their sensitivity in capturing the change in toxic effects caused by ABR treatment.

3.4. Pollutant Removals in Municipal Wastewater via ABR. ABR treatment resulted in the favorable removal of fecal coliform in all samples (Figure 6a). For PE, 50 g/L ABR removed fecal coliform effectively by >99.6% (>log 2.43) with 100 g/L by ∼99.96% (>log 3.38). Both SE and post-UV-treated effluents had lower initial fecal coliforms, but the 50 and 100 g/L ABR treatment resulted in concentrations below detection limits. This result suggests that ABR has the potential to act as a disinfectant, but further testing of its efficacy on the inactivation of specific pathogens is required. Although bauxite residue has been integrated with nanosize zinc oxide and assessed for its disinfection properties,[58] it has not been explored as a disinfectant while functioning as an adsorbent. Possible mechanisms of disinfection include the increase in coliform die-off due to the increase in pH (pH > 9), inhibition by metals that leach out from ABR, and trapping of bacteria in ABR or in the metal complexes forming polyvalent cations such as Al from ABR. Overall, there is currently limited evidence on the disinfection properties of bauxite residues, but ABR contains various oxides (iron, aluminum, titanium), some of which can have bactericidal effects.[59]

The results also demonstrated the effective removal of nutrients by the ABR (Figure 6a). For instance, total ammonia-N was reduced from 26 to 8 mg/L (69% removal) and 9.5 mg/L (63% removal) in PE samples using 50 and 100 g/L ABR, respectively. Although removals were observed (19−25%), the values obtained for SE and post-UV effluent treatment with ABR were smaller potentially due to the lower initial ammonia-N concentration (0.16 mg/L). Increasing the ABR dosage to 100 g/L slightly decreased the removal of ammonia-N likely due to the rise in pH, which alters the form of ammonia-N in water. At pH > 10, NH_4^+ converts to its unionized ammonia and is less favorable for removal via adsorption. Similarly, Phillips et al.[40] reported the adsorption of NH_4^+ onto bauxite residue decreased with increasing pH.

Furthermore, the concentrations of total phosphorus in all three samples were reduced to ≪1 mg/L after ABR treatment. For PE, total phosphorus was decreased from 4.7 to 0.097 mg/L (98% removal) and 0.13 mg/L (97% removal) by 50 and 100 g/L ABR, respectively. Similar removals were observed for SE. Although the initial concentration (0.18 mg/L) was already below the discharge limit for the post-UV effluent, ABR also resulted in additional removals with concentrations reaching ∼0.040 mg/L. Phosphate removal has been observed for bauxite residues (at 500 g/L dosage[44]) and was linked to ligand-exchange mechanism on the surface[60] or electrostatic interaction of negatively charged species (such as phosphate) on the cation (Ca^{2+} or Mg^{2+}) present on the surface.[44] Again, our work is a proof-of-concept study, and the dosage of ABR for phosphorus removal will require more optimization.

By contrast, the concentrations of TSS and BOD were found to be higher after ABR treatment (Figure 6a). This result suggested that the current experimental conditions (e.g., jar testing and mixing intensity, settling time) were inadequate for solid removal. Further pilot testing that couples ABR treatment with a solid separation unit process is important to determine operational parameters for TSS reduction. The increase in BOD was not surprising as acetic acid used for neutralization is a simple, carbon-based molecule assimilable by bacteria. Acetic acid can be used as an external carbon source to the activated sludge process. Thus, incorporating the ABR treatment process with biological treatment unit or installing the ABR treatment and neutralization as a pretreatment option would potentially decrease the residual BOD concentration. Acetic acid can undergo biological oxidation by up to 82% in freshwater after 10 d.[61] Given that this study is a preliminary attempt to determine the potential of ABR as a sorbent alternative, it will be important to assess how the pH increase and the release of metals from ABR can interfere with other treatment plant unit processes (e.g., biological treatment, settling/sedimentation).

3.4.1. Biological Activity in Municipal Wastewater Effluents. The overall trend in estrogenicity and mutagenicity was similar to that observed for the OSPW such that the biological activities were reduced after treatment (Figure 6b). Although a 6-fold decrease in cytotoxicity was observed after the 50 and 100 g/L ABR treatment in PE, cytotoxicity increased by 5 and 3 times when 50 and 100 g/L ABR were applied to the SE and post-UV effluent, respectively. By contrast, there was very little change in cytotoxicity observed when a higher dose of ABR was applied (i.e., 100 g/L). This observation suggested that the increase in cytotoxicity may not be directly related to the leaching of metals, especially Al; otherwise, the cytotoxicity would have likely increased with the ABR dosage applied. Conversely, there is the possibility that the metal complexes formed are less toxic than the original species.[62] Also, the cytotoxic effects observed for municipal wastewater were different from those for OSPW (increased cytotoxicity at an increased ABR dosage), indicating that differences in water matrices may also be an influencing parameter.

4. CONCLUSIONS

This study examined the potential of using ABR as a potential option for the treatment of OSPW and municipal wastewater. ABR was characterized as a magnetic and charged material (PZC = pH ∼ 5) consisting of 1.33% carbon in the bulk material, with highly porous particles that are either carbon-rich or metal oxide-rich. Our results further show that ABR removed AEOs, estrogenicity, and mutagenicity from the OSPW but led to an increase in cytotoxicity. The adsorption of AEOs followed the pseudo-second-order kinetics, suggesting that chemisorption might be the dominant removal mechanism. The ABR performance in the OSPW treatment is similar to those of other nonactivated carbon adsorbent alternatives reported in the literature (i.e., petroleum coke and biochar). The addition of acetic acid after treatment also decreased the leaching of metals (especially Al) from ABR. Furthermore, ABR effectively removed fecal coliforms, total phosphorus, total ammonia-N, estrogenicity, and mutagenicity in all three

https://doi.org/10.1021/acsomega.4c06699
ACS Omega 2024, 9, 45251−45262

types of municipal effluents studied (primary, secondary, and post-UV effluents). BOD and TSS increased, suggesting that additional testing is required to assess the feasibility of ABR as either a pre- or post-treatment process as well as its impact on existing unit processes such as sedimentation/settling tanks. Overall, optimization of ABR dosages (ideally, sub-g/L range) and expanding the assessment of ABR on a larger scale will enable the comprehensive assessment of its combined effect on existing WWTP processes. The magnetic properties of ABR also allow for the recovery of magnetite, which can be completed after wastewater treatment. Given the ubiquity of bauxite residue, there is a large potential for ABR as an economically viable sorbent alternative, further transforming this waste product into a valuable resource. Future studies can inform the regeneration and reuse of ABR to maximize its potential.

■ ASSOCIATED CONTENT

Supporting Information

The Supporting Information is available free of charge at https://pubs.acs.org/doi/10.1021/acsomega.4c06699.

Experimental setup, material characterization, methylene blue experimental results, and additional water quality effluent data (PDF)

■ AUTHOR INFORMATION

Corresponding Author

Maricor J. Arlos − *Department of Civil and Environmental Engineering, University of Alberta, Edmonton, Alberta T6G 1H9, Canada; Department of Civil and Environmental Engineering, University of Waterloo, Waterloo, Ontario N2L 3G1, Canada;* orcid.org/0000-0001-6365-3955; Email: arlos@ualberta.ca, mjarlos@uwaterloo.ca

Authors

Fei Cheng − *Department of Civil and Environmental Engineering, University of Alberta, Edmonton, Alberta T6G 1H9, Canada*

Jingya Pang − *Department of Civil and Environmental Engineering, University of Alberta, Edmonton, Alberta T6G 1H9, Canada*

Scott Berggren − *GRÖN Holding Corporation, Toronto, Ontario M5H 3S1, Canada*

Himanshu Tanvar − *Material Science and Engineering, Worcester Polytechnic Institute, Worcester, Massachusetts 01609, United States;* orcid.org/0000-0001-7329-7464

Brajendra Mishra − *Material Science and Engineering, Worcester Polytechnic Institute, Worcester, Massachusetts 01609, United States*

Complete contact information is available at: https://pubs.acs.org/10.1021/acsomega.4c06699

Notes

The authors declare no competing financial interest.

■ ACKNOWLEDGMENTS

This work was financially supported by Mitacs Accelerate (75%) and GRÖN Holding Corp. (25%). Additional funding was obtained from the Canada First Research Excellence Fund as a part of the University of Alberta's Future Energy Systems (FES) research initiative. Additional funding from the NSERC Discovery Grant (NSERC RGPIN-2021-02412) was also obtained to support this work. We also gratefully acknowledge the help and support of the University of Alberta (Dr. Ania Ulrich, Dr. Mohamed Gamal El-Din) and the NanoFAB fabrication and characterization facility from the University of Alberta and the industrial partners (GRÖN) for this project. We thank Bing Lin from EPCOR for assisting us with the acquisition of effluent samples.

■ REFERENCES

(1) Kirwan, L. J.; Hartshorn, A.; McMonagle, J. B.; Fleming, L.; Funnell, D. Chemistry of bauxite residue neutralisation and aspects to implementation. *Int. J. Miner. Process.* **2013**, *119*, 40−50.

(2) Khanna, R.; Konyukhov, Y.; Zinoveev, D.; Jayasankar, K.; Burmistrov, I.; Kravchenko, M.; Mukherjee, P. S. Red mud as a secondary resource of low-grade iron: A global perspective. *Sustainability* **2022**, *14* (3), 1258.

(3) International Aluminum Institute Sustainable Bauxite Residue Management Guidance—International Aluminium Institute. https://international-aluminium.org/resource/sustainable-bauxite-mining-guidelines-second-edition-2022-2/ (accessed April 7).

(4) Tang, W.; Khavarian, M.; Yousefi, A. Red Mud. In *Sustainable Concrete Made with Ashes and Dust from Different Sources: Materials, Properties and Applications*; Siddique, R.; Belarbi, R., Eds.; Woodhead Publishing, 2021.

(5) Mayes, W. M.; Burke, I.; Gomes, H.; Anton, Á.; Molnár, M.; Feigl, V.; Ujaczki, É. Advances in understanding environmental risks of red mud after the Ajka spill, Hungary. *J. Sustain. Metall.* **2016**, *2*, 332−343.

(6) Ujaczki, É.; Feigl, V.; Molnár, M.; Vaszita, E.; Uzinger, N.; Erdélyi, A.; Gruiz, K. The potential application of red mud and soil mixture as additive to the surface layer of a landfill cover system. *J. Environ. Sci.* **2016**, *44*, 189−196.

(7) Rubinos, D.; Spagnoli, G.; Barral, M. T. Assessment of bauxite refining residue (red mud) as a liner for waste disposal facilities. *Int. J. Min., Reclam. Environ.* **2015**, *29* (6), 433−452.

(8) Mukiza, E.; Zhang, L.; Liu, X.; Zhang, N. Utilization of red mud in road base and subgrade materials: A review. *Resour., Conserv. Recycl.* **2019**, *141*, 187−199.

(9) Zeng, H.; Lyu, F.; Sun, W.; Zhang, H.; Wang, L.; Wang, Y. Progress on the industrial applications of red mud with a focus on China. *Minerals* **2020**, *10* (9), 773.

(10) Dimas, D. D.; Giannopoulou, I. P.; Panias, D. Utilization of alumina red mud for synthesis of inorganic polymeric materials. *Miner. Process. Extr. Metall. Rev.* **2009**, *30* (3), 211−239.

(11) Cardenia, C.; Balomenos, E.; Panias, D. Iron recovery from bauxite residue through reductive roasting and wet magnetic separation. *J. Sustain. Metall.* **2019**, *5*, 9−19.

(12) Tanvar, H.; Mishra, B. Extraction of Titanium, Aluminum, and Rare Earth Values from Upgraded Bauxite Residue. *J. Sustain. Metall.* **2023**, *9* (2), 665−677.

(13) Wang, Y.; Zhang, T.-a.; Lyu, G.; Guo, F.; Zhang, W.; Zhang, Y. Recovery of alkali and alumina from bauxite residue (red mud) and complete reuse of the treated residue. *J. Cleaner Prod.* **2018**, *188*, 456−465.

(14) Paradis, M.; Duchesne, J.; Lamontagne, A.; Isabel, D. Long-term neutralisation potential of red mud bauxite with brine amendment for the neutralisation of acidic mine tailings. *Appl. Geochem.* **2007**, *22* (11), 2326−2333.

(15) Domingues, E.; Assunção, N.; Gomes, J.; Lopes, D. V.; Frade, J. R.; Quina, M. J.; Quinta-Ferreira, R. M.; Martins, R. C. Catalytic efficiency of red mud for the degradation of olive mill wastewater through heterogeneous Fenton's process. *Water* **2019**, *11* (6), 1183.

(16) Barca, C.; Scanu, D.; Podda, N.; Miche, H.; Poizat, L.; Hennebert, P. Phosphorus removal from wastewater by carbonated bauxite residue under aerobic and anoxic conditions. *J. Water Process Eng.* **2021**, *39*, No. 101757.

(17) Zhang, S.; Guo, S.; Li, A.; Liu, D.; Sun, H.; Zhao, F. Low-cost bauxite residue-MoS2 possessing adsorption and photocatalysis ability

https://doi.org/10.1021/acsomega.4c06699
ACS Omega 2024, 9, 45251−45262

for removing organic pollutants in wastewater. *Sep. Purif. Technol.* **2022**, *283*, No. 120144.
(18) Yang, W.; Hussain, A.; Zhang, J.; Liu, Y. Removal of elemental mercury from flue gas using red mud impregnated by KBr and KI reagent. *Chem. Eng. J.* **2018**, *341*, 483−494.
(19) Simair, M. C.; Parrott, J. L.; le Roux, M.; Gupta, V.; Frank, R. A.; Peru, K. M.; Ajaero, C.; McMartin, D. W.; Headley, J. V. Treatment of oil sands process affected waters by constructed wetlands: Evaluation of designs and plant types. *Sci. Total Environ.* **2021**, *772*, No. 145508.
(20) Li, C.; Fu, L.; Stafford, J.; Belosevic, M.; Gamal El-Din, M. The toxicity of oil sands process-affected water (OSPW): A critical review. *Sci. Total Environ.* **2017**, *601−602*, 1785−1802.
(21) Nazari, E.; Roy, T. M.; Strong, O. K.; Vreugdenhil, A. J. Adsorption of Naphthenic Acids from Oil Sand Process-Affected Water (OSPW) Using Commercially Viable Petcoke-Sourced Activated Carbon. In Conference of MetallurgistsSpringer, 2022; pp 251−254.
(22) Quinlan, P. J.; Tam, K. C. Water treatment technologies for the remediation of naphthenic acids in oil sands process-affected water. *Chem. Eng. J.* **2015**, *279*, 696−714.
(23) Gupta, V. K.; Suhas; Ali, I.; Saini, V. Removal of rhodamine B, fast green, and methylene blue from wastewater using red mud, an aluminum industry waste. *Ind. Eng. Chem. Res.* **2004**, *43* (7), 1740−1747.
(24) Gupta, V. K.; Ali, I.; Saini, V. Removal of chlorophenols from wastewater using red mud: an aluminum industry waste. *Environ. Sci. Technol.* **2004**, *38* (14), 4012−4018.
(25) Aydın, S.; Bedük, F.; Ulvi, A.; Aydın, M. E. Simple and effective removal of psychiatric pharmaceuticals from wastewater treatment plant effluents by magnetite red mud nanoparticles. *Sci. Total Environ.* **2021**, *784*, No. 147174.
(26) Genç-Fuhrman, H.; Tjell, J. C.; McConchie, D. Adsorption of arsenic from water using activated neutralized red mud. *Environ. Sci. Technol.* **2004**, *38* (8), 2428−2434.
(27) Deihimi, N.; Irannajad, M.; Rezai, B. Characterization studies of red mud modification processes as adsorbent for enhancing ferricyanide removal. *J. Environ. Manage.* **2018**, *206*, 266−275.
(28) Zouboulis, A. I.; Kydros, K. A. Use of red mud for toxic metals removal: the case of nickel. *J. Chem. Technol. Biotechnol.* **1993**, *58* (1), 95−101.
(29) Zhao, Z.; Wang, B.; Feng, Q.; Chen, M.; Zhang, X.; Zhao, R. Recovery of nitrogen and phosphorus in wastewater by red mud-modified biochar and its potential application. *Sci. Total Environ.* **2023**, *860*, No. 160289.
(30) Bourgin, M.; Beck, B.; Boehler, M.; Borowska, E.; Fleiner, J.; Salhi, E.; Teichler, R.; von Gunten, U.; Siegrist, H.; McArdell, C. S. Evaluation of a full-scale wastewater treatment plant upgraded with ozonation and biological post-treatments: Abatement of micro-pollutants, formation of transformation products and oxidation by-products. *Water Res.* **2018**, *129*, 486−498.
(31) Schollée, J. E.; Hollender, J.; McArdell, C. S. Characterization of advanced wastewater treatment with ozone and activated carbon using LC-HRMS based non-target screening with automated trend assignment. *Water Res.* **2021**, *200*, No. 117209.
(32) Svahn, O.; Borg, S. Assessment of full-scale 4th treatment step for micro pollutant removal in Sweden: Sand and GAC filter combo. *Sci. Total Environ.* **2024**, *906*, No. 167424.
(33) Neuwald, I. J.; Muschket, M.; Seelig, A. H.; Sauter, D.; Gnirss, R.; Knepper, T. P.; Reemtsma, T.; Zahn, D. Efficacy of activated carbon filtration and ozonation to remove persistent and mobile substances—A case study in two wastewater treatment plants. *Sci. Total Environ.* **2023**, *886*, No. 163921.
(34) Gostu, S. Investigation of carbon-based reductant, low-temperature process for conversion of hematite in red-mud to magnetite-ProQuest MSc Thesis, Colorado School of Mines, 2016. Available at https://www.proquest.com/docview/1766582114?pq-origsite=gscholar&fromopenview=true&sourcetype=Dissertations%20&%20Theses (accessed Aug 06, 2024).
(35) Barrow, K.; Escher, B. I.; Hicks, K. A.; König, M.; Schlichting, R.; Arlos, M. J. Water quality monitoring with in vitro bioassays to compare untreated oil sands process-affected water with unimpacted rivers. *Environ. Sci.: Water Res. Technol.* **2023**, *9* (8), 2008−2020.
(36) Tanvar, H.; Mishra, B. Comprehensive utilization of bauxite residue for simultaneous recovery of base metals and critical elements. *Sustainable Mater. Technol.* **2022**, *33*, No. e00466.
(37) Sahoo, T. R.; Prelot, B. Adsorption Processes for the Removal of Contaminants from Wastewater: The Perspective Role of Nanomaterials and Nanotechnology. In *Nanomaterials for the Detection and Removal of Wastewater Pollutants*; Elsevier, 2020; pp 161−222.
(38) Arlos, M. J.; Liang, R.; Hatat-Fraile, M. M.; Bragg, L. M.; Zhou, N. Y.; Servos, M. R.; Andrews, S. A. Photocatalytic decomposition of selected estrogens and their estrogenic activity by UV-LED irradiated TiO2 immobilized on porous titanium sheets via thermal-chemical oxidation. *J. Hazard. Mater.* **2016**, *318*, 541−550.
(39) Liu, Y.; Naidu, R. Hidden values in bauxite residue (red mud): Recovery of metals. *Waste Manage.* **2014**, *34* (12), 2662−2673.
(40) Phillips, I. R.; Chen, C. Surface charge characteristics and sorption properties of bauxite-processing residue sand. *Soil Res.* **2010**, *48* (1), 77−87.
(41) Ren, J.; Chen, J.; Guo, W.; Yang, B.; Qin, X.-p.; Du, P. Physical, chemical, and surface charge properties of bauxite residue derived from a combined process. *J. Cent. South Univ.* **2019**, *26* (2), 373−382.
(42) Bjelopavlic, M.; Newcombe, G.; Hayes, R. Adsorption of NOM onto Activated Carbon: Effect of Surface Charge, Ionic Strength, and Pore Volume Distribution. *J. Colloid Interface Sci.* **1999**, *210* (2), 271−280.
(43) Thommes, M.; Kaneko, K.; Neimark, A. V.; Olivier, J. P.; Rodriguez-Reinoso, F.; Rouquerol, J.; Sing, K. S. Physisorption of gases, with special reference to the evaluation of surface area and pore size distribution (IUPAC Technical Report). *Pure Appl. Chem.* **2015**, *87* (9−10), 1051−1069.
(44) Cusack, P. B.; Healy, M. G.; Ryan, P. C.; Burke, I. T.; O'Donoghue, L. M.; Ujaczki, É.; Courtney, R. Enhancement of bauxite residue as a low-cost adsorbent for phosphorus in aqueous solution, using seawater and gypsum treatments. *J. Cleaner Prod.* **2018**, *179*, 217−224.
(45) Huang, W.; Wang, S.; Zhu, Z.; Li, L.; Yao, X.; Rudolph, V.; Haghseresht, F. Phosphate removal from wastewater using red mud. *J. Hazard. Mater.* **2008**, *158* (1), 35−42.
(46) Martins, Y. J. C.; Almeida, A.; Viegas, B.; do Nascimento, R.; Ribeiro, N. d. P. Use of red mud from amazon region as an adsorbent for the removal of methylene blue: process optimization, isotherm and kinetic studies. *IInt. J. Environ. Sci. Technol.* **2020**, *17*, 4133−4148.
(47) Wang, S.; Boyjoo, Y.; Choueib, A.; Zhu, Z. Removal of dyes from aqueous solution using fly ash and red mud. *Water Res.* **2005**, *39* (1), 129−138.
(48) Hu, Z.-P.; Gao, Z.-M.; Liu, X.; Yuan, Z.-Y. High-surface-area activated red mud for efficient removal of methylene blue from wastewater. *Adsorpt. Sci. Technol.* **2018**, *36* (1−2), 62−79.
(49) Kazak, O.; Eker, Y. R.; Akin, I.; Bingol, H.; Tor, A. A novel red mud@ sucrose based carbon composite: Preparation, characterization and its adsorption performance toward methylene blue in aqueous solution. *J. Environ. Chem. Eng.* **2017**, *5* (3), 2639−2647.
(50) Cao, J.; Wang, Y.; Yan, Z.; Li, G. Polystyrene microspheres-templated preparation of hierarchical porous modified red mud with high rhodamine B dye adsorption performance. *Micro Nano Lett.* **2014**, *9* (4), 229−231.
(51) Mestre, A. S.; Campinas, M.; Viegas, R. M.; Mesquita, E.; Carvalho, A. P.; Rosa, M. J. Activated carbons in full-scale advanced wastewater treatment. *Adv. Mater. Sustainable Environ. Rem.* **2022**, 433−475.
(52) Mandal, A.; Dey, B. B.; Das, S. K. Thermodynamics, kinetics, and isotherms for phenol removal from wastewater using red mud. *Water Pract.Technol.* **2020**, *15* (3), 705−722.
(53) Bhuiyan, T. I.; Tak, J. K.; Sessarego, S.; Harfield, D.; Hill, J. M. Adsorption of acid-extractable organics from oil sands process-

https://doi.org/10.1021/acsomega.4c06699
ACS Omega 2024, 9, 45251−45262

affected water onto biomass-based biochar: metal content matters. *Chemosphere* **2017**, *168*, 1337−1344.
(54) Zubot, W.; MacKinnon, M. D.; Chelme-Ayala, P.; Smith, D. W.; El-Din, M. G. Petroleum coke adsorption as a water management option for oil sands process-affected water. *Sci. Total Environ.* **2012**, *427*−*428*, 364−372.
(55) Zubot, W.; An, Z.; Benally, C.; Gamal El-Din, M. Treatment of oil sands process water using petroleum coke: Field pilot. *J. Environ. Manage.* **2021**, *289*, No. 112407.
(56) Barrow, K. In Vitro Bioassay Monitoring to Assess Baseline Conditions Prior to Potential Discharge of Treated Oil Sands Process Water in Receiving Aquatic Environments. Thesis, University of Alberta: Edmonton, 2022.
(57) Yue, S.; Ramsay, B. A.; Wang, J.; Ramsay, J. A. Biodegradation and detoxification of naphthenic acids in oil sands process affected waters. *Sci. Total Environ.* **2016**, *572*, 273−279.
(58) Li, J.; Zhu, Q.; Su, Y.; Wang, D.; Xing, Z.; Fang, L. High-efficiency bacteriostatic material modified by nano zinc oxide and polyelectrolyte diallyl dimethylammonium chloride based on red mud. *Colloids Surf., B* **2019**, *177*, 260−266.
(59) Pachaiappan, R.; Rajendran, S.; Show, P. L.; Manavalan, K.; Naushad, M. Metal/metal oxide nanocomposites for bactericidal effect: A review. *Chemosphere* **2021**, *272*, No. 128607.
(60) Akhurst, D. J.; Jones, G. B.; Clark, M.; McConchie, D. Phosphate removal from aqueous solutions using neutralised bauxite refinery residues (Bauxsol). *Environ. Chem.* **2006**, *3* (1), 65−74.
(61) Verschueren, K. *Handbook of Environmental Data on Organic Chemicals*; LWW, 1985.
(62) Qin, R.; Lillico, D.; How, Z. T.; Huang, R.; Belosevic, M.; Stafford, J.; Gamal El-Din, M. Separation of oil sands process water organics and inorganics and examination of their acute toxicity using standard in-vitro bioassays. *Sci. Total Environ.* **2019**, *695*, No. 133532.

https://doi.org/10.1021/acsomega.4c06699
ACS Omega 2024, 9, 45251−45262